

# Measurement and analysis of angle-resolved scatter from small particles in a cylindrical microchannel

Murugesan Venkatapathi, Gérald Grégori, Kathy Ragheb, J. Paul Robinson, and E. Dan Hirleman

Scatter of a two-dimensional Gaussian beam of a rectangular cross section by individual particles suspended in a fluid in a cylindrical channel is modeled by using a full-wave approach. First, the internal and scattered fields associated with the cylindrical channel and the two-dimensional Gaussian beam are computed. The spatial variations of the computed electromagnetic field inside the channel indicate that particles and cells of sizes relevant to flow cytometry are subjected to essentially plane-wave illumination, and hence Lorenz-Mie theory is applicable for spherical particles. Further, it is assumed that the perturbation of the electromagnetic field in the channel that is due to the presence of a particle is negligible, allowing us to ignore the interactive scatter of the particle and the channel (they are electromagnetically uncoupled). This approximation is valid when the particle intercepts a small fraction of the total energy inside the channel and when the particle or cell has a low relative refractive index. Measurements of scatter from the channel agree with the analytical model and are used to determine the location of detectors to measure scatter from particles in the channel. Experimental results of accumulated scatter from single latex spheres flowing in the channel show good agreement with computed results, thereby validating the internal field and uncoupled scatter models. © 2006 Optical Society of America

*OCIS code:* 290.5820.

## 1. Introduction

In many single-particle characterizing systems the particles being studied flow through a microchannel while they are probed by a laser beam. If scatter is one of the measured parameters, a single-scatter measurement is used for detection and for an estimation of the variability in size and optical properties of the particles. On the other hand, an angle-resolved scatter measurement is a much more accurate indicator for the size, shape, and complex refractive index of a particle. A few configurations of such instruments exist for angular light-scattering measurements of particles,<sup>1-3</sup> in

which a laser beam of dimensions much smaller than those of the channel is aligned with the axis of the channel used for probing the particles. But in typical single-particle analysis applications, the laser beams are incident at an angle (90° typically) with the axis of the channel because of the disadvantages of using a single laser beam aligned with the axis of the channel. This is especially true when these particles must be sorted based on their properties or when multiple laser beams have to be used separately to study different properties of particles and cells. Such scatter measurements in general cannot be represented by an isolated particle in a laser beam, since the change of characteristics and dimensions of the laser beam inside the channel (internal field) and resultant scatter due to multiple reflections within the channel (electromagnetic coupling) have to be included. A rigorous solution of the electromagnetic scattering problem of an arbitrary particle in a cylindrical channel is too difficult a problem today, and hence the validity of isolated-particle models is studied in this paper with relevance to single-particle systems such as flow cytometers.

To accomplish this, we model the internal fields of a channel irradiated by a normally incident two-dimensional Gaussian beam. The perturbation of this internal field, and hence the perturbation of scatter from the channel due to the presence of the particle, can be assumed to be negligible when the relative re-

---

M. Venkatapathi (mvenkata@purdue.edu), E. D. Hirleman, K. Ragheb, and J. Robinson are with Purdue University, West Lafayette, Indiana 47907. M. Venkatapathi and E. D. Hirleman are with the Department of Mechanical Engineering. K. Ragheb and J. P. Robinson are with the Department of Basic Medical Sciences, and J. P. Robinson is also with the Department of Biomedical Engineering and the Bindley Bioscience Center. G. Grégori is with Laboratoire de Microbiologie, Géochimie et Ecologie Marines, Centre National de la Recherche Scientifique, Unité Mixte de Recherche 6117, 163 Avenue de Luminy, Case 90, 13288 Marseille Cedex 9, France.

Received 27 September 2005; revised 30 November 2005; accepted 1 December 2005; posted 5 December 2005 (Doc. ID 65057).

0003-6935/06/102222-10\$15.00/0

© 2006 Optical Society of America

fractive index of the particle in the medium is not high and when the cross-sectional dimensions of the particle are much less than that of the representative length scale of the internal-field's beam cross section.<sup>4</sup> This means that the scatter from the flow channel does not vary much in the presence of a small particle within, and hence the analytical scatter model of the channel makes it convenient to locate the detectors for the angular-scatter measurement of particles in which scatter from the flow channel is less than the detection limit of the sensors. This also allows us to ignore the interactive scatter–electromagnetic coupling due to multiple reflections of the scatter from particles in the channel. Also to be explored is whether the internal field can be represented by regularly shaped beams for which scattering theory of particles can be used. In such cases in which electromagnetic coupling can indeed be ignored and the internal field can be approximated as a regularly shaped beam, scattering theory can be applied to study the particles flowing in channels. The measured scatter from the particle in the far field can then be expected to match that of the particle in the internal field with the corresponding geometric optical approximations to the scattered partial waves across the different boundaries between the particle and the detector.

Although the solution for scattering of Gaussian laser sheets by infinite cylinders was developed a number of years ago,<sup>5–7</sup> the scattering of two-dimensional Gaussian beams on infinite cylinders was solved<sup>8–10</sup> only in the last decade with modifications<sup>11</sup> to the separability theorem of linear partial-differential equations.<sup>12</sup> Typically these flow channels are etched in a large bulk material, such as a block of glass, that is much larger than the channel itself. Hence, in this study, all angular measurements are in the apparent positions with corresponding geometric optical approximations ( $k = nk'$ , where  $n$  is the refractive index of the medium and  $k'$  is the free-space wavenumber) unless mentioned otherwise. The purpose of this paper is to lay out the analytical methods used in such an approximation and to show its validity with experiments that measure angle-resolved accumulated scatter from small spheres flowing in the channel.

This paper has five sections. Section 1 provides an introduction. Section 2 presents the theoretical methods used in the calculation of the scatter from the flow channel and the internal fields. Section 3 presents the analytical results of the scatter, internal fields, and experimental measurements of scatter from the flow channel. In Section 4 the analytical calculation of scatter accumulated from a distribution of single latex spheres and its measurement is briefly explained and a comparison of the measurements with the analytical results for the spheres is presented. Section 5 concludes the paper.

## 2. Scattering of a Two-Dimensional Gaussian Beam by a Circular Cylindrical Channel

The cylindrical channel can be modeled as an infinite cylinder irradiated with a Gaussian beam when  $L \gg \omega$ , where  $L$  is the length of the cylinder and  $\omega$  is

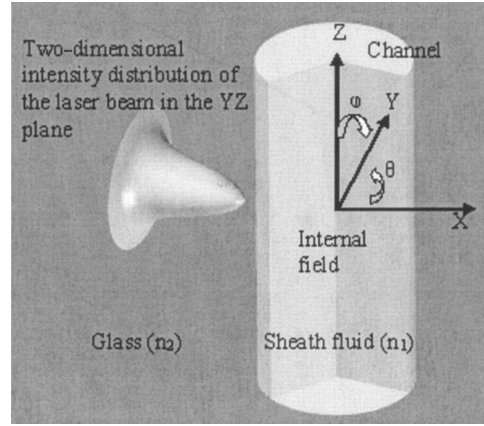


Fig. 1. Channel is represented as a homogeneous dielectric cylinder with the incident laser beam propagating along the  $x$  axis. The refractive indices of glass and sheath fluid are  $n_1$  and  $n_2$ , respectively.

the  $1/e$  width of the incident Gaussian beam. The dimensions of the laser beam propagating inside the bulk glass (calculated in the absence of the channel) at the focus  $(x_0, y_0, 0)$  are assumed to be known, and Fig. 1 shows the coordinate system used.

The incident electric-field vector or the incident magnetic field vector can be polarized in the  $xy$  (horizontal) plane, which we denote as  $\epsilon$  and  $\mu$  polarizations, respectively, as in Lock.<sup>13</sup> In the cylindrical coordinate system ( $r^2 = x^2 + y^2$ ), the field vectors in the former case are

$$\begin{aligned} \mathbf{E}(r, \theta, z) &= \mathbf{e}_z \times \nabla \psi^\epsilon(r, \theta, z), \\ \mathbf{B}(r, \theta, z) &= (i/\omega) \nabla \times [\mathbf{e}_z \times \nabla \psi^\epsilon(r, \theta, z)], \end{aligned} \quad (1)$$

and the corresponding potential can be written as

$$\begin{aligned} \psi_{\text{inc}}^\epsilon(r, \theta, z) &= \int_{-\infty}^{+\infty} dh \sum_{l=-\infty}^{l=+\infty} \frac{i^{l+1}}{k} E_0 A_l(h) \\ &\times J_l[kr(1-h^2)^{1/2}] \exp(ikhz) \exp(il\theta), \end{aligned} \quad (2)$$

where  $A_l(h)$  is the partial-wave beam-shape coefficients,  $h$  is a spectrum that depends on the beam shape,  $l$  is the partial wavenumber, and  $J_l$  are the Bessel functions. Using Eqs. (1) and (2), we can write the beam-shape coefficients as

$$\begin{aligned} A_l(h) &= \frac{(-i)^l k}{(2\pi)^2 (1-h^2) J_l[kr(1-h^2)^{1/2}]} \\ &\times \int_{-\infty}^{+\infty} dz \int_0^{2\pi} d\theta \exp(-ikhz) \exp(-il\theta) \\ &\times cB_{z,\text{inc}}(r, \theta, z)/E_0. \end{aligned} \quad (3)$$

If the beam is  $\mu$  polarized,

$$\mathbf{B}(r, \theta, z) = (m/c) \mathbf{e}_z \times \nabla \psi^\mu(r, \theta, z),$$

$$\mathbf{E}(r, \theta, z) = (-ic/m\omega) \nabla \times [\mathbf{e}_z \times \nabla \psi^\mu(r, \theta, z)], \quad (4)$$

and the radiation potential and corresponding beam-shape coefficients are given by

$$\psi_{\text{inc}}^\mu(r, \theta, z) = \int_{-\infty}^{+\infty} dh \sum_{l=-\infty}^{l=+\infty} \frac{i^{l+1}}{k} E_0 B_l(h) \times J_l[kr(1-h^2)^{1/2}] \exp(ikhz) \exp(il\theta), \quad (5)$$

$$B_l(h) = \frac{(-i)^l k}{(2\pi)^2 (1-h^2) J_l[kr(1-h^2)^{1/2}]} \times \int_{-\infty}^{+\infty} dz \int_0^{2\pi} d\theta [\exp(-ikhz) \times \exp(-il\theta)] E_{z,\text{inc}}(r, \theta, z) / E_0. \quad (6)$$

### A. Calculating Beam-Shape Coefficients

The calculation of beam-shape coefficients and its justification is nontrivial,<sup>14-16</sup> and we use the angular spectrum of the plane-wave model to determine the beam-shape coefficients.<sup>13</sup> Let the  $z$  component of the  $\mu$  polarized incident Gaussian beam at  $x_0$  be given by

$$\mathbf{E}_{z,\text{inc}}(x_0, y, z) = E_0 \exp\left[\frac{-(y-y_0)^2 - z^2}{\omega_0^2}\right]. \quad (7)$$

Equation (7) can be represented as a Fourier integral and be generalized to all  $x$  by

$$E_{z,\text{inc}}(x, y, z) = \frac{E_0 \omega_0^2}{4\pi} \int_{-\infty}^{+\infty} k dh_y \times \int_{-\infty}^{+\infty} k dh_z \exp\left(\frac{-h_y^2}{4s^2}\right) \times \exp\left(\frac{-h_z^2}{4s^2}\right) \exp[ikh_x(x-x_0)] \times \exp[ikh_x(y-y_0)] \exp(ikh_z z), \quad (8)$$

where

$$s = 1/k\omega_0. \quad (9)$$

The above beam is an exact solution to Maxwell's equation if

$$h_x = (1 - h_y^2 - h_z^2)^{1/2}, \quad (10)$$

$$\nabla \cdot \mathbf{E}_{\text{inc}} = 0. \quad (11)$$

The beam-shape coefficient  $B_l(h)$  can now be calculated by substituting Eq. (8) into Eq. (6) even though the integral is not integrable analytically. The term

$\exp(-h_y^2/4s^2)$  can be expanded as a series, and terms higher than quadratic can be ignored if  $h_y^2 \ll 1$ . As was observed before,<sup>13</sup> this approximation is valid for beams that are not tightly focused. For example, when  $\omega_0 = 3\lambda$ , the half-width in  $h$  space is  $s \sim 0.053$  and  $\exp(-h_y/4s^2) \sim 3 * 10^{-4}$  if  $h_y^2 = 0.1$ , and hence only a small fraction of the incident energy is neglected. For our applications  $\omega_0 > 20\lambda$ , and this is a very good approximation. Thus

$$B_l(h) = \frac{1}{2\pi^{1/2} s (1-h^2) [1 - 2is^2 k x_0 (1-h^2)^{-1/2}]^{1/2}} \times \exp\left(\frac{-h}{4s^2}\right) \exp[-ik(1-h^2)^{1/2} x_0] \times \exp\left\{\frac{-s^2[l(1-h^2)^{-1/2} + ky_0]^2}{1 - 2is^2 k x_0 (1-h^2)^{-1/2}}\right\}, \quad (12)$$

$$A_l(h) = 0.$$

Similarly the beam-shape coefficients for an  $\epsilon$ -polarized Gaussian beam are

$$A_l(h) = \frac{1}{2\pi^{1/2} s (1-h^2) [1 - 2is^2 k x_0 (1-h^2)^{-1/2}]^{1/2}} \times \exp\left(\frac{-h}{4s^2}\right) \exp[-ik(1-h^2)^{1/2} x_0] \times \exp\left\{\frac{-s^2[l(1-h^2)^{-1/2} + ky_0]^2}{1 - 2is^2 k x_0 (1-h^2)^{-1/2}}\right\}, \quad (13)$$

$$B_l(h) = 0.$$

### B. Calculating the Scattered and Internal Fields

The scattered radiation potentials are expanded as

$$\psi_{\text{scat}}^\epsilon(r, \theta, z) = - \int_{-\infty}^{+\infty} dh \sum_{l=-\infty}^{l=+\infty} \frac{i^{l+1}}{k} E_0 \alpha_l(h) \times H_l^{(1)}[kr(1-h^2)^{1/2}] \exp(ikhz) \exp(il\theta),$$

$$\psi_{\text{scat}}^\mu(r, \theta, z) = - \int_{-\infty}^{+\infty} dh \sum_{l=-\infty}^{l=+\infty} \frac{i^{l+1}}{k} E_0 \beta_l(h) \times H_l^{(1)}[kr(1-h^2)^{1/2}] \exp(ikhz) \exp(il\theta) \quad (14)$$

for the two polarizations correspondingly, and  $H_l^{(1)}$  are the Hankel functions of first kind. The partial-wave scattering amplitudes are  $\alpha_l(h)$  and  $\beta_l(h)$ , and the internal field can be similarly expanded into

$$\psi_{\text{int}}^\epsilon(r, \theta, z) = \int_{-\infty}^{+\infty} dh' \sum_{l=-\infty}^{l=+\infty} \frac{i^{l+1}}{k} E_0 n \gamma_l(h') \times J_l[nkr(1-h'^2)^{1/2}] \exp(ikh'z) \exp(il\theta),$$

$$\psi_{\text{int}}^{\mu}(r, \theta, z) = \int_{-\infty}^{+\infty} dh' \sum_{l=-\infty}^{l=+\infty} \frac{i^{l+1}}{k} E_0 n \delta_l(h') \\ \times J_l[nkr(1-h'^2)^{1/2}] \exp(ikh'z) \exp(il\theta), \quad (15)$$

where

$$h' = h/n \quad (16)$$

and  $\gamma_l(h)$  and  $\delta_l(h)$  are the partial-wave interior amplitudes,  $n$  is the relative refractive index of the cylinder or channel ( $n = n_1/n_2$ ), and the radius of the channel is given by  $a$ . The field-continuity relations<sup>9</sup> then result in

$$\alpha_l(h) = a_l(h)A_l(h) + q_l(h)B_l(h), \\ \beta_l(h) = -q_l(h)A_l(h) + b_l(h)B_l(h), \quad (17)$$

for the scattering amplitudes. For the interior amplitudes, they are given by

$$\gamma_l(h') = c_l(h)A_l(h) + p_l(h)B_l(h), \\ \delta_l(h') = -np_l(h)A_l(h) + d_l(h)B_l(h), \quad (18)$$

where

$$\alpha_l(h) = \frac{U_2 W_1 - n U_3 W_3}{W_2 W_1 - n W_3^2}, \\ b_l(h) = \frac{U_1 W_2 - n U_3 W_3}{W_2 W_1 - n W_3^2}, \\ q_l(h) = \frac{2nlh(y^2 - x^2)}{\pi x^2 y^2} \frac{J_l^2(y)}{W_2 W_1 - n W_3^2}, \\ c_l(h) = \frac{-2inx}{\pi y^2} \frac{W_1}{W_2 W_1 - n W_3^2}, \\ d_l(h) = \frac{-2inx}{\pi y^2} \frac{W_2}{W_2 W_1 - n W_3^2}, \\ p_l(h) = \frac{-2nx}{\pi y^2} \frac{W_3}{W_2 W_1 - n W_3^2}, \quad (19)$$

$$x \equiv ka(1-h^2)^{1/2}, \\ y \equiv nka[1-(h^2/n^2)]^{1/2}, \quad (20)$$

$$U_1 = \frac{n^2 x}{y} J_l(x) J_l'(y) - J_l'(x) J_l(y),$$

$$U_2 = \frac{nx}{y} J_l(x) J_l'(y) - n J_l'(x) J_l(y),$$

$$U_3 = \frac{hl(y^2 - x^2)}{xy^2} J_l(x) J_l(y),$$

$$W_1 = \frac{n^2 x}{y} H_l^{(1)}(x) J_l'(y) - H_l^{(1)'}, \\ \times (x) J_l(y),$$

$$W_2 = \frac{nx}{y} H_l^{(1)}(x) J_l'(y) - n H_l^{(1)'}, \\ \times (x) J_l(y),$$

$$W_3 = \frac{hl(y^2 - x^2)}{xy^2} H_l^{(1)}(x) J_l(y). \quad (21)$$

The far-zone scattered fields are obtained by substituting Eqs. (14) and (16) into Eqs. (1) and (4) and by taking the  $r \rightarrow \infty$  limit. The corresponding scattered intensity vector is<sup>13</sup>

$$\lim_{r \rightarrow \infty} \mathbf{I}_{\text{scat}}(r, \theta, z) = \text{Re} \left\{ \frac{\mathbf{E}_{\text{scat}}^* \times \mathbf{B}_{\text{scat}}}{2\mu_0 c} \right\} \\ = \frac{2}{\pi k r} \left( \frac{E_0^2}{2\mu_0 c} \right) \text{Re} [ (T_2^* T_4 + T_3^* T_1) \mathbf{e}_r \\ + (T_5^* T_4 - T_3^* T_6) \mathbf{e}_\theta + (T_5^* T_1 + T_2^* T_6) \mathbf{e}_z ], \quad (22)$$

where

$$T_1(r, \theta, z) = \int_{-\infty}^{+\infty} dh \sum_{l=-\infty}^{l=+\infty} (1-h^2)^{1/4} \beta_l(h) \\ \times \exp[ikr(1-h^2)^{1/2}] \exp(ikhz) \exp(il\theta),$$

$$T_2(r, \theta, z) = \int_{-\infty}^{+\infty} dh \sum_{l=-\infty}^{l=+\infty} (1-h^2)^{1/4} \alpha_l(h) \\ \times \exp[ikr(1-h^2)^{1/2}] \exp(ikhz) \exp(il\theta),$$

$$T_3(r, \theta, z) = \int_{-\infty}^{+\infty} dh \sum_{l=-\infty}^{l=+\infty} (1-h^2)^{3/4} \beta_l(h) \\ \times \exp[ikr(1-h^2)^{1/2}] \exp(ikhz) \exp(il\theta),$$

$$T_4(r, \theta, z) = \int_{-\infty}^{+\infty} dh \sum_{l=-\infty}^{l=+\infty} (1-h^2)^{3/4} \alpha_l(h) \\ \times \exp[ikr(1-h^2)^{1/2}] \exp(ikhz) \exp(il\theta),$$

$$T_5(r, \theta, z) = \int_{-\infty}^{+\infty} dh \sum_{l=-\infty}^{l=+\infty} h(1-h^2)^{1/4} \beta_l(h) \\ \times \exp[ikr(1-h^2)^{1/2}] \exp(ikhz) \exp(il\theta),$$

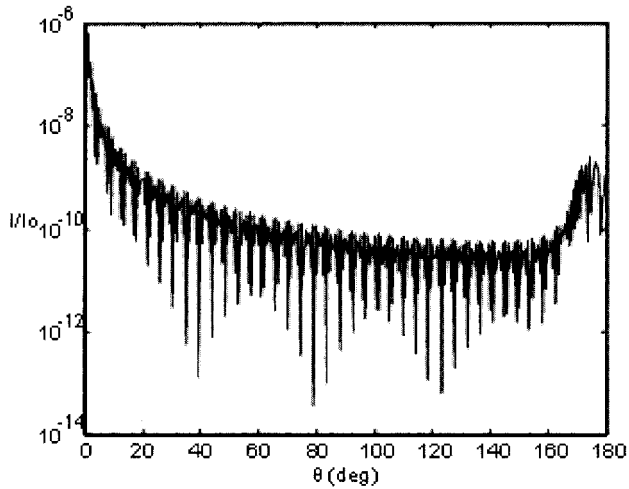


Fig. 2. Variation of the scattered intensity normalized by  $I_0$  [infinite cylinder with peak intensity of the laser beam at  $(x_0, y_0)$ ] as a function of  $\theta$  at a radial distance of 25 mm and  $\phi = 90^\circ$ .  $z = 0$ ,  $a = 125 \mu\text{m}$ ,  $n_1 = 1.33$ , and  $n_2 = 1.5$ .

$$T_6(r, \theta, z) = \int_{-\infty}^{+\infty} dh \sum_{l=-\infty}^{l=+\infty} h(1-h^2)^{1/4} \alpha_l(h) \times \exp[ikr(1-h^2)^{1/2}] \exp(ikhz) \exp(il\theta). \quad (23)$$

Similarly, the internal fields are obtained by substituting Eqs. (15) and (18) into Eqs. (1) and (4). In case the incident Gaussian beam has different beam widths in the  $y$  and  $z$  directions, caution should be used in scaling the  $y$  or  $z$  axis in Eq. (7) to represent the incident beam profile and similarly scaling the spatial distribution of scattering amplitude in Eq. (22). This is because Eq. (7) is only a local approximation at  $x_0$  and hence does not have a direct scaling relationship with Eq. (22). In fact, reducing the beam dimension in Eq. (7) results in an expansion of the spatial distribution of scattering amplitude in the far field [Eq. (22)]. In such a case, the  $S_z$  and  $S_y$  (half-widths in  $h$  space) are to be defined separately for the  $y$  and  $z$  directions in Eqs. (8) and (9) and carried over to Eqs. (12) and (13).

### 3. Results of Scattered and Internal Fields

The analytical method presented above can be used to model scatter from parametrized flow channels. The scattered intensity in the specific case of a channel made of a material with a refractive index of 1.5 ( $n_2$ ) filled with a fluid of refractive index 1.33 ( $n_1$ ) is shown in Fig. 2. The laser beam is normally incident on a channel of radius 125  $\mu\text{m}$  and has a two-dimensional Gaussian profile with beam widths of 125 and 16  $\mu\text{m}$  in the  $y$  and  $z$  directions, respectively, at a focus of  $E_0^u/E_0^e = 0.33$  and  $\lambda = 488 \text{ nm}$  in free space. The results are plotted as a function of angle with the  $x$  axis in the  $xy$  plane ( $\theta$ ). For the purposes of this paper, we consider only the case in which the beam is focused at  $y_0 = z_0 = x_0 = 0$ , which is the center of the channel.

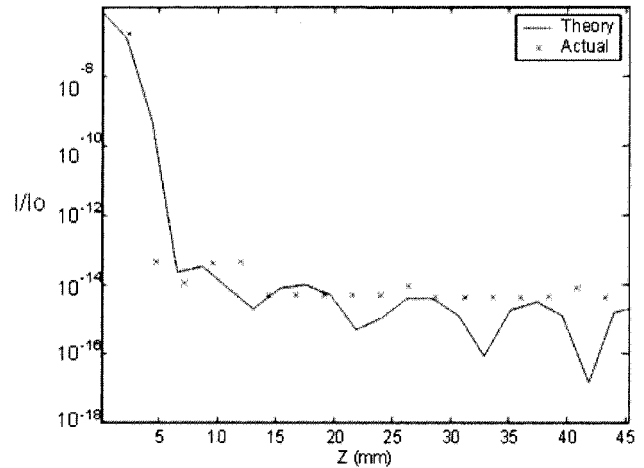


Fig. 3. Variation of the scattered intensity from the channel normalized by  $I_0$  [the peak intensity of the laser beam at  $(x_0, y_0)$ ] as a function of  $z$  at  $\theta = 0^\circ$ .  $a = 125 \mu\text{m}$ ,  $r = 250 \text{ mm}$ ,  $n_1 = 1.33$ , and  $n_2 = 1.5$ .

Figure 3 shows the variation of the scatter intensity of the flow channel with  $z$  and the actual measurements for the above case. The measured intensities shown were corrected for variation of the solid angle as a function of the apparent  $z$  positions (corrected for refraction) outside the bulk glass. The dimension of the detectors (S8865-64, Hamamatsu Corporation) at each  $z$  location is 0.8 mm and 2.4 mm in the  $y$  and  $z$  directions. We observe that the scattered intensity from the flow channel falls off rapidly with increasing  $|z|$ . This is true for normally illuminated infinite cylinders in which most of the scattered energy is in the  $xy$  plane, whereas for spheres and many other particles the scattered energy is spread over large angles away from the  $xy$  plane.<sup>17</sup> Thus the detectors can then be located where scatter from the cylindrical channel is lower than the detection limit of the scatter sensors, while that of the particles is within its range.

Calculation of the internal field within the cylindrical channel is essential to the model of scatter from particles flowing in the channel. Though the internal field has been modeled for large beams incident on small cylinders (using incident plane waves) before,<sup>18,19</sup> the case of incident Gaussian beams gives us interesting results. The analytical results show that the internal field maintains a Gaussian profile in the  $z$  direction but not in the  $y$  direction [see Figs. 5(a) and 5(b)]. This is because the partial waves of the laser beam do not change directions significantly in the  $z$  direction, but they do in the  $\theta$  direction.<sup>13</sup> This can also be inferred by plotting the beam-shape coefficients ( $B$ ,  $\gamma$ ,  $\delta$ ) as a function of  $l$  and  $h$  (Fig. 4). While the incident- and internal-beam-shape coefficients have a similar Gaussian distribution with  $h$ , their distributions with  $l$  are quite different, indicating a change in profile in the  $y$  direction.

Moreover, it is interesting that the internal field (more polarized in the  $z$  direction) is different from the incident beam (more polarized in  $y$ ) in polariza-

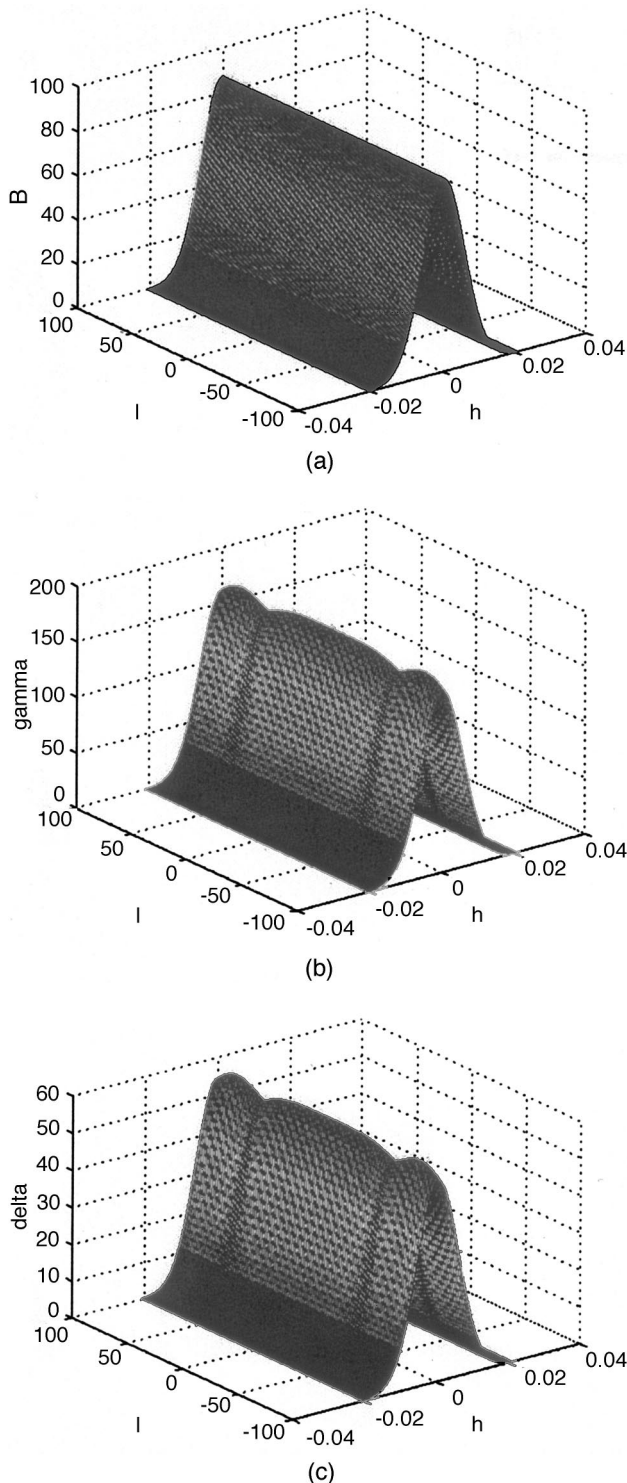


Fig. 4. Amplitudes of (a)  $B$ , (b)  $E_0^\epsilon$ , (c)  $\delta E_0^\mu$  as a function of  $h$  and  $l$ .

tion and amplitude as shown in Fig. 5. Knowledge of the internal energy and the polarization ratio (especially in the case of nonspherical particles) is important, because it changes the apparent cross section and angular intensity distribution significantly, depending on the internal energy and orientation of the electric field vector with respect to the particle. In

flow cytometers, particles are hydrodynamically focused, and the longer dimension is nearly always aligned with  $z$ . Hence knowledge of the orientation of the electric field vector helps us with the exact calculation of scatter from each particle.

#### 4. Accumulated Scatter from a Distribution of Spheres

The internal fields can now be used to analytically calculate the scatter from a latex sphere inside the channel by using Lorenz–Mie theory (LMT).<sup>20</sup> To assume the spheres are in a plane-wave field polarized in the  $z$  direction seems reasonable since the variation of the electric field inside the channel (according to a Gaussian half-width of  $16\ \mu\text{m}$  in the  $z$  direction and  $20\ \mu\text{m}$  in the  $y$  direction) across the particles used in this study is very small, provided the above-shown distributions are nearly uniform at all  $x$  inside the cylinder. Also, the phase of  $E_z$  should be plane-wave-like with the corresponding wavelength for us to use LMT for the theoretical model. The two-dimensional field distribution and phase distribution were hence calculated and are shown in Fig. 5. Although there are small variations in the amplitude of  $E_z$  with  $x$  and  $y$  and in the phase of  $E_z$  with  $y$ , the internal field can be approximated as a plane wave propagating in the  $x$  direction with  $\lambda = 488/n_1$  nm. This approximation is valid for calculating scatter by small particles but tends to diverge from experimental results as the particles become larger.

As we accumulate the scatter for multiple spheres flowing in the channel in this study, we have to consider the distribution in diameters of the spheres to compute the aggregate scatter. Two groups of latex spheres (polystyrene microspheres; Polysciences, Inc.) with a normal distribution in size and mean diameters of  $4.369\ \mu\text{m}$  ( $\sigma = 0.287$ ) and of  $1.71\ \mu\text{m}$  ( $\sigma = 0.089$ ) with a refractive index 1.59 were used in this study (where  $\sigma$  is the standard deviation of the distribution). The aggregate scatter from such a distribution of spheres is calculated by

$$I_s(\theta, \phi) = \int_{d=0}^{\infty} A_d I_{sd}(\theta, \phi) dd, \quad (24)$$

where  $I_{sd}(\theta, \phi)$  represents the scattered intensity of a sphere of diameter  $d$ ,  $\phi$  is the angle with a positive  $z$  axis,  $\theta$  is the angle with an  $x$  axis in the  $xy$  plane, and  $A_d$  is the probability of the presence of the sphere of diameter  $d$  in the group.  $A_d$  is given by

$$A_d = \frac{1}{\sigma\sqrt{2\pi}} \exp[-(d - d_0)^2/2\sigma^2], \quad (25)$$

where  $d_0$  is the mean diameter of the group.

As shown in the experimental setup (Fig. 6), the spherical mirror (assumed reflectivity of 1) results in an antisymmetric addition of intensities (assuming uncorrelated reflection from the mirror on the average as the particle moves across the beam), and hence the measured scatter intensity is given by

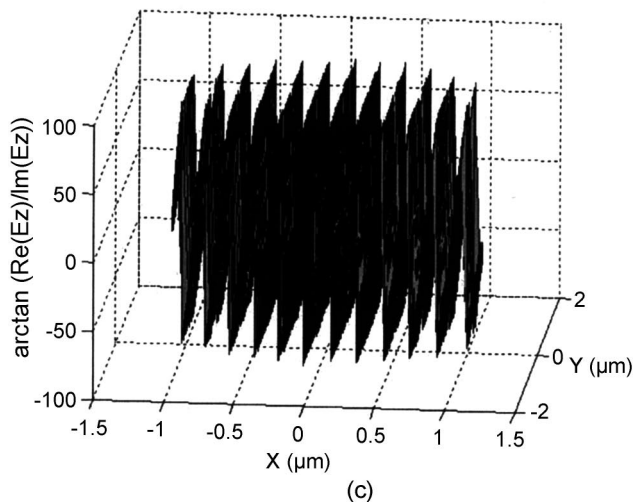
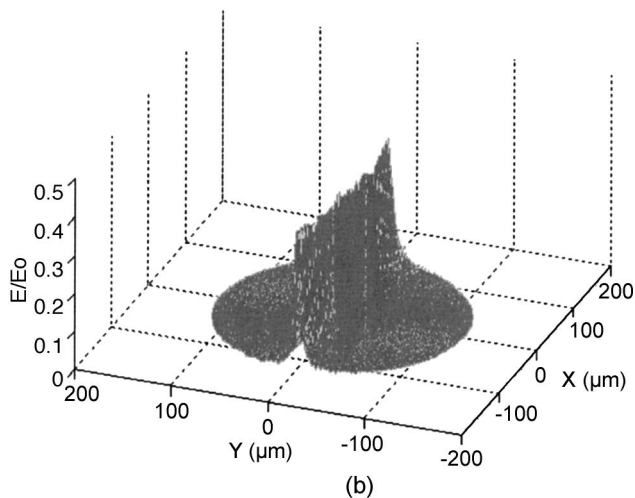
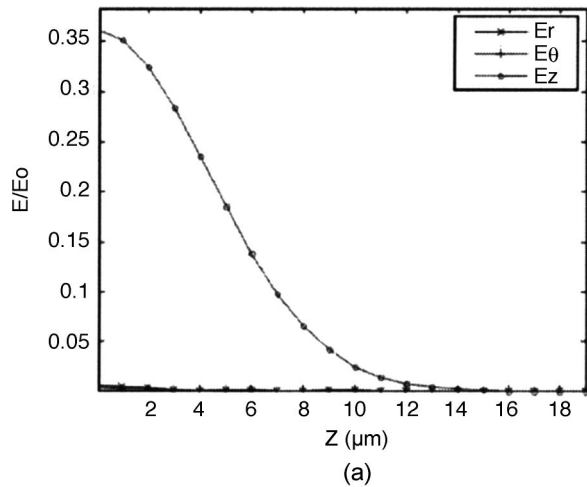


Fig. 5. (a) Amplitudes of the internal electric field distribution as a function of  $z$  (where  $E_0^h + E_0^e = E_0$ ), (b) Distribution of the amplitude of  $E_z$  in the  $xy$  plane, (c) Phase of  $E_z$  in the  $xy$  plane.  $n_1 = 1.33$ ,  $n_2 = 1.5$ ,  $a = 125 \mu\text{m}$ ,  $r = 0$ ,  $z = 0$ .

$$I_m(\theta, \phi) = I_s(\theta, \phi) + I_s(180^\circ + \theta, 180^\circ + \phi), \quad (26)$$

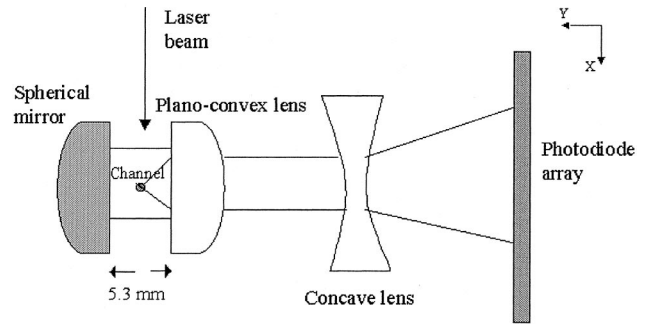


Fig. 6. Top view of the experimental setup used to measure the intensity of scattered light from particles flowing in the channel. (Drawing is not to scale.)

where  $I_m(\theta, \phi)$  is the measured scattered intensity of the sphere and the analytical scatter calculations for the distribution of spheres obtained with LMT are given by  $I_s(\theta, \phi)$ ,  $I_s(180^\circ + \theta, 180^\circ + \phi)$ .

In the experimental setup shown in Fig. 6, the particles flow at high speeds one by one across the laser through the channel etched in the glass. The flow system used is that of a flow cytometer (Elite, Beckman Coulter, Inc.), an instrument that is specially designed for extracting small single particles from a colloidal sample and directing them across a laser beam one by one. The flow system is designed such that the particles flow through the center of the channel where the internal electromagnetic field is at maximum. The scattered field is reflected back from the spherical mirror on one side into a system of two lenses, which spreads the light onto a scatter detector that has 64 photodiodes in a linear array with a pixel size of  $800 \mu\text{m} \times 800 \mu\text{m}$  (S8865-64, Hamamatsu Corporation). This mirror is added to double the weak scatter signals at  $\theta \sim 90^\circ$ . The scattered intensities of particles were measured as a function of  $\theta$  at  $\phi = 70^\circ$ ; as most of the scattered energy from the channel is distributed in the range  $100^\circ \geq \phi \geq 80^\circ$ . In the above experimental setup there is an additional negligible perturbation of the internal field of the channel due to the scatter from the spheres reflected back from the spherical mirror. This energy reflected from the mirror is very small compared with the energy incident on the spheres ( $\sim 10^{-3}$ ), since most of the scattered energy from the particles is in the forward direction along the laser.<sup>18</sup>

Also to be considered is the phase relationship of the scatter reflected from the mirror ( $225^\circ \geq \theta \leq 315^\circ$ ) with respect to the scatter from the particle in the range  $45^\circ \geq \theta \leq 135^\circ$  to see whether these are uncorrelated on the average as the particle moves across the beam inside the channel (measurements at constant  $\phi = 70^\circ$ ). This is necessary to determine whether we can use the addition of the intensities of scatter reflected from the mirror and the scatter from the particle, as done in our analytical model. If the location of the particle is nominally fixed in space at the center of a perfectly spherical mirror, the apparent angular location of the detectors with respect to

the particle does not change. As the particle moves across the laser beam—internal field inside the channel in the  $z$  direction, the change in angular location ( $d\phi$ ) of the particle with respect to the mirror and hence the detectors ( $d\phi = \omega/R \sim 0.008$  rad, ratio of beam width in the  $z$  direction to the radius of curvature of the mirror) is indeed negligible in this case. But the phase relationship between the scatter reflected from the mirror and the scatter from the particle ( $45^\circ \geq \theta \leq 135^\circ$ ) has a sensitivity to the change in the distance of the particle from the center of the mirror of the order of  $\lambda$ . Hence, as the sphere moves in the  $z$  direction across the laser beam ( $z$  dimension  $\sim 35\lambda$  in this case), this phase relationship between the scatter from the spheres and the scatter reflected from the mirror varies as a function of the  $z$  position of the sphere and the measurement location  $\phi$ . Any off centricity in the  $x$  and  $y$  directions creates a similar variation in this phase relationship as a function of the  $x$  and  $y$  positions of the sphere and the measurement location  $\theta$ . Hence the movement of the spheres across the beam in the  $z$  direction, the additional off centricity of particles in the  $x$  and  $y$  directions, and the aberrations in the shape of mirror all result in a continuous variation in the phase of the scattered field reflected from the mirror with respect to the scatter from the particle ( $45^\circ \geq \theta \leq 135^\circ$ ). Also, in the case of accumulated scatter from multiple spheres, the random variations of the off centricity of each sphere in the  $x$  and  $y$  directions (of the order of  $\lambda$ ) in such flow systems decreases the correlation between the scatter reflected from the mirror and the scatter from the spheres on average by a factor of  $N^{1/2}$  (where  $N$  is the number of spheres from which scatter is accumulated). Hence the scatter reflected from the mirror ( $225^\circ \geq \theta \leq 315^\circ$ ) is uncorrelated with the scatter from the spheres ( $45^\circ \geq \theta \leq 135^\circ$ ) on average, and the detector senses the sum of these intensities. However, caution is advised with applying this assumption to single-particle measurements or to small  $N$ , as its validity depends on the beam width and the uncertainty in the paths of the spheres in the  $x$  and  $y$  directions. Furthermore, in actual single-particle applications, the use of this mirror might be unnecessary when fewer and more sensitive detectors can be used for the scatter measurements.

In actual experiments in such a flow system, there is always a small probability that there are two particles in the laser beam—internal field simultaneously or that particles flow in parts of the channel where the internal field energy and resulting scatter is too small for the particles to be detected.<sup>21</sup> The number of particles flowing per second across the laser beam in these experiments was approximately 10,000, and the corresponding integration time for angle-resolved scatter measurements was approximately 0.5 s (triggered by the single forward-scatter measurements used for particle detection and counting). Since we have performed aggregate scatter measurements of single particles flowing in the channel, it is imperative to convince ourselves that there is a low proba-

bility of having more than one particle in the laser beam simultaneously. This is all the more important in this case, since a concentrated sample was used at high flow rates to minimize any ambient optical noise that could affect the measurements.

Hence the same sets of sample latex spheres used for the scatter measurements were run across the laser at the same flow conditions, and the approximate percentage of events in which two or more spheres are involved are determined. This process involves the assumption that the internal field has a Gaussian profile in the  $z$  direction. This has been known to be the case in flow cytometry, since the scattered intensity of the particles flowing across the channel has been observed to have a Gaussian temporal profile. But this assumption was shown analytically in this paper, and we use this fact to show that the probability of finding more than one particle in the laser beam simultaneously was in fact low. The total scattered energy and the peak and maximum of scattered intensity due to each particle are measured for each event and particle. If there is only one particle in the laser beam, the relationship between these two quantities is the one between the Gaussian amplitude and the integral of the Gaussian curve. That is, the total scattered energy has a logarithmic relationship with the peak intensity when the velocity of the particles across the Gaussian internal electric field distribution is constant (same flow conditions). This is used to determine the number of events that do not satisfy this relationship and thereby provides an estimate of the probability of there being more than one particle in the laser beam. Also, the distribution of the intensity peaks and scattered energies by themselves give us a qualitative idea of the size distribution of the spheres and of the ratio of single-particle events to total events. This procedure was repeated multiple times with the same group of spheres to determine this probability. Figure 7 shows the results of one such experiment for both the 1.71 and 4.369  $\mu\text{m}$  sphere groups in which 5000 spheres were analyzed. These experiments demonstrated that the maximum probability of having more than one particle in the beam was 0.052 and 0.029 for those two groups of spheres, respectively.

Figure 8 shows the analytical results of the normalized accumulated scatter for latex spheres with a distribution of diameters as mentioned above and the actual scatter measurements in the range  $45^\circ \leq \theta \leq 90^\circ$ . The intensity measurements were corrected for the variation of the projected solid angle of the different detectors and the refraction of the scattered partial waves across the channel surface. As mentioned before, the measurements agree reasonably well with the analytical model of accumulated scatter from the corresponding latex spheres in the internal field of the channel. The larger divergence of the measurements from the analytical model in the case of the 4.369  $\mu\text{m}$  spheres is explained by their larger size, resulting in a small but nonnegligible perturba-



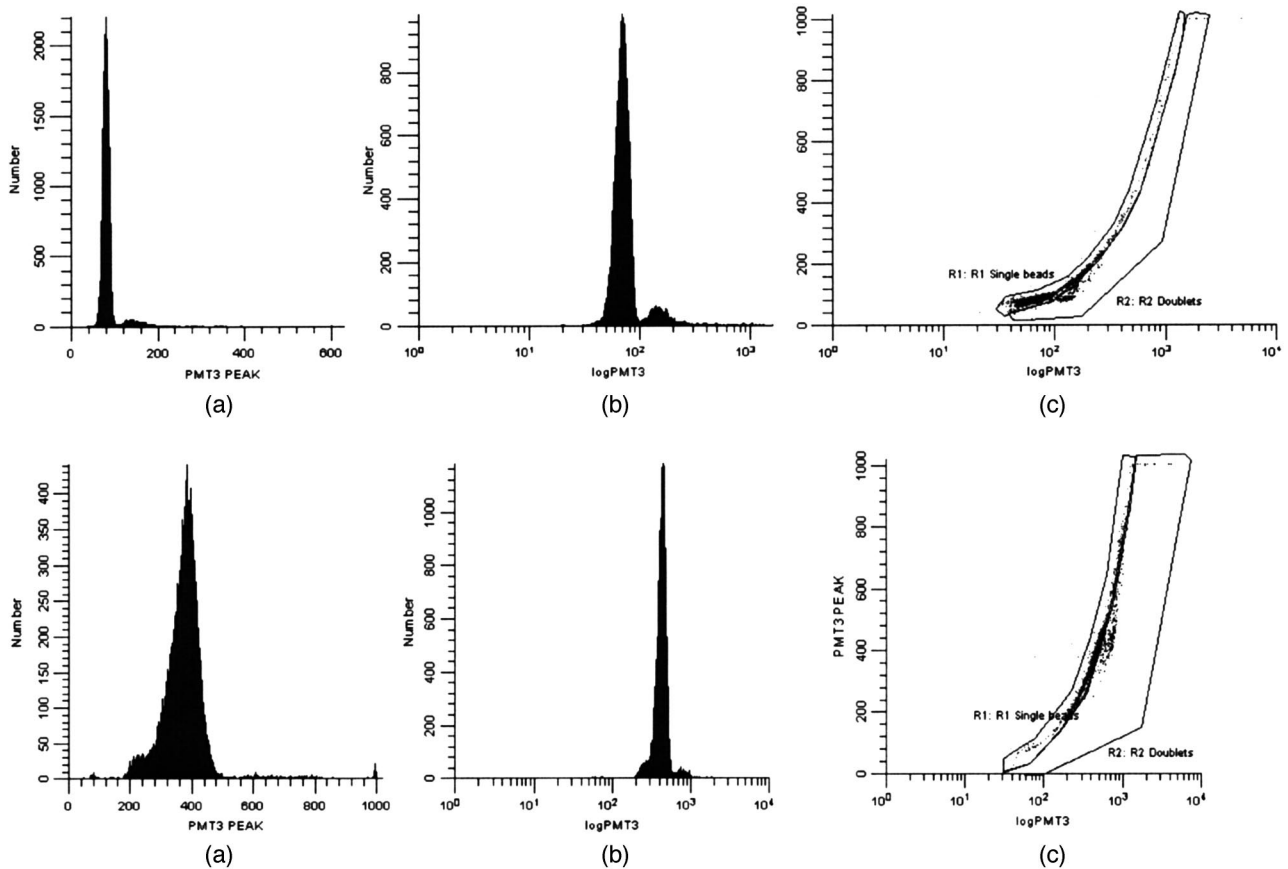


Fig. 7. (a) Number of spheres versus peak intensity (arbitrary units), (b) number of spheres versus total scattered energy (arbitrary units), (c) peak intensity versus total scattered energy (region R1 represents single spheres in the laser beam) for (top) 1.71  $\mu\text{m}$  spheres and (bottom) 4.369  $\mu\text{m}$  spheres.

tion of the internal field (higher electromagnetic coupling with the channel).

### 5. Conclusion

With the recent developments in scattering theory of Gaussian beams, it is possible to model the internal and scattered fields of the cylindrical flow channels used in single-particle analysis systems. Hence it is possible to go beyond the models that assume an isolated particle in the laser beam to better understand the scattering of particles flowing in a channel. The fact that the internal field of the channel can be different from the incident laser beam in its energy distribution and polarization is an important factor to be considered in the modeling of scatter from particles in a flow channel. The phase and amplitude distributions inside the channel show that the scatter can be approximated by using plane-wave incidence and Gaussian laser sheets in the case of small particles. This model is useful in the case of microchannels and laser beams used in flow cytometry ( $50 \mu\text{m} < a < 200 \mu\text{m}$ ) that are not large enough for geometrical approximation of internal fields as the laser beam itself. These models of internal fields also indicate that in designing such flow systems, the internal fields have to be studied for the range of laser beams used. This is because as the size parameter ( $ka$ ) of the

channel is reduced, the internal fields diverge from the laser beam, nonuniformity of internal energy increases, and excitation of specific modes<sup>18</sup> results in an increase of energy along the circumference of the

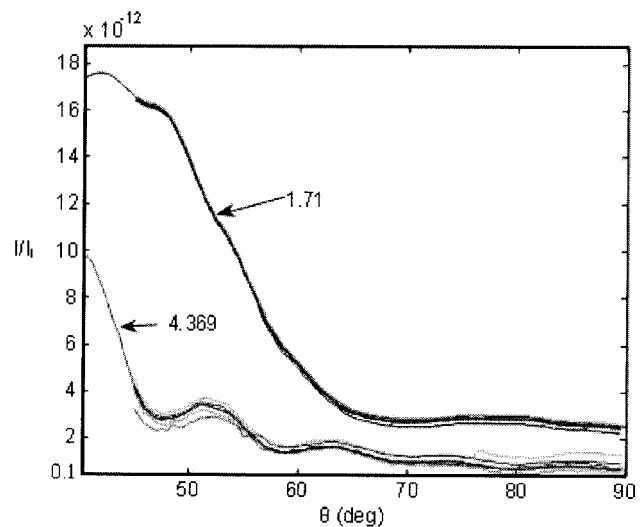


Fig. 8. Scattered intensity from a distribution of single latex spheres normalized by  $I_i$  ( $1/e^2$  value of the peak intensity inside the channel).

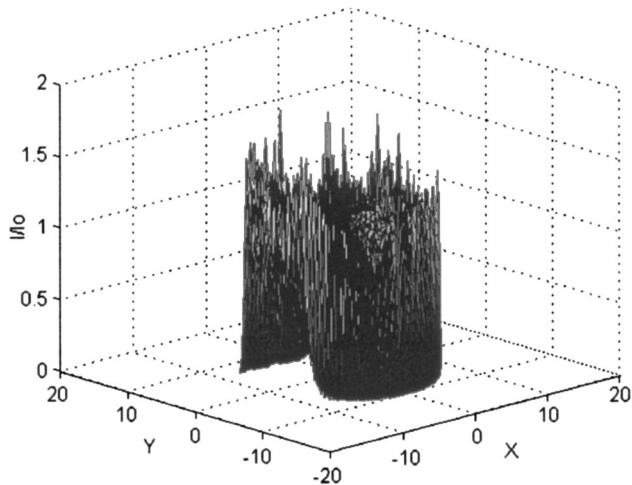


Fig. 9. Internal energy distribution at  $z = 0$  for a channel of diameter  $20 \mu\text{m}$ , with a fluid illuminated by a normally incident  $z$ -polarized,  $16 \mu\text{m} \times 20 \mu\text{m}$  Gaussian laser beam with a free-space wavelength of  $488 \text{ nm}$ .  $a = 10 \mu\text{m}$ ,  $n_1 = 1.33$ ,  $n_2 = 1.5$ .

channel (shown in Fig. 9). This increase in intensity and spreading of the energy may reduce relative electromagnetic coupling between the particles and the channel, but owing to the nonuniformity of the energy distribution, the internal field cannot be represented by regularly shaped beams.

The exact range of sizes for which the internal field can be approximated by plane waves and Gaussian laser sheets depends on the size parameter of the channel and on the incident-beam dimensions. Once the internal fields are known, uniformity of its amplitude and its phase distribution dictates the validity of the use of plane waves and Gaussian laser sheets. Hence internal field models of channels are useful in studying the degree of interaction of particles in channels with the incident energy and in exploring the validity of scattering theory in the study of scatter from these particles.

In cases in which such an approximation is valid, the models of scatter from the flow channel and the particles themselves are useful in designing experiments for measuring the angle-resolved scatter from particles. Using these models it has been observed that for the flow channels and laser beams (beam width in the  $y$  direction is dictated by the diameter of the channel) used in flow cytometry ( $500 < ka < 2000$ ,  $450 \text{ nm} < \lambda < 650 \text{ nm}$ ), the representative length scale of the beam cross section in the  $xy$  plane is at least  $20 \mu\text{m}$  with plane-wave-Gaussian-laser-sheet-like phase and amplitude distributions. This means that for typical cells (relative refractive indices  $< 1.1$ ) flowing in such channels, if their dimension is less than  $\sim 10 \mu\text{m}$ , the existing analytical models that ignore the electromagnetic coupling between channel and particles are reasonable.

## References

1. A. V. Chernyshev, V. I. Prots, A. A. Doroshkin, and V. P. Maltsev, "Measurement of scattering properties of individual

- particles with a scanning flow cytometer," *Appl. Opt.* **34**, 6045–6311 (1995).
2. A. N. Shvalov, I. V. Surovtsev, A. V. Chernyshev, J. T. Soini, and V. P. Maltsev, "Particle classification from light scattering with the scanning flow cytometer," *Cytometry* **37**, 215–220 (1999).
3. E. D. Hirlleman and C. F. Bohren, "Optical particle sizing: an introduction by the feature editors," *Appl. Opt.* **30**, 4685–4687 (1991).
4. J. A. Lock, "Interpretation of extinction in Gaussian-beam scattering," *J. Opt. Soc. Am. A* **12**, 929–938 (1995).
5. N. G. Alexopoulos and P. K. Park, "Scattering of waves with normal amplitude distribution from cylinders," *IEEE Trans. Antennas Propag.* **AP-20**, 216–217 (1972).
6. T. J. Kojima and Y. Yanagiuchi, "Scattering of an offset two-dimensional Gaussian beam wave by a cylinder," *J. Appl. Phys.* **50**, 41–46 (1979).
7. S. Kozaki, "Scattering of a Gaussian beam by a homogeneous dielectric cylinder," *IEEE Trans. Antennas Propag.* **AP-30**, 881–887 (1982).
8. G. Gouesbet and G. Gréhan, "Interaction between a Gaussian beam and an infinite cylinder with the use of non- $\Sigma$ -separable potentials," *J. Opt. Soc. Am. A* **11**, 3261–3273 (1994).
9. G. Gouesbet and G. Gréhan, "Interaction between shaped beams and an infinite cylinder, including a discussion of Gaussian beams," *Part. Part. Syst. Charact.* **11**, 299–308 (1994).
10. G. Gouesbet, "Interaction between Gaussian beams and infinite cylinders by using the theory of distributions," *J. Opt. (Paris)* **26**, 225–239 (1995).
11. G. Gouesbet, "The separability theorem revisited with applications to light scattering theory," *J. Opt. (Paris)* **26**, 123–125 (1995).
12. P. M. Morse and H. Feshbach, *Methods of Theoretical Physics, Part I* (McGraw-Hill, 1953).
13. J. A. Lock, "Scattering of a diagonally incident focused Gaussian beam by an infinitely long homogeneous circular cylinder," *J. Opt. Soc. Am. A* **14**, 640–652 (1997).
14. J. A. Lock and G. Gouesbet, "Rigorous justification of the localized approximation to the beam-shape coefficients in generalized Lorenz-Mie theory. I. On-axis beams," *J. Opt. Soc. Am. A* **11**, 2503–2515 (1994).
15. G. Gouesbet and J. A. Lock, "Rigorous justification of the localized approximation to the beam-shape coefficients in generalized Lorenz-Mie theory. II. Off-axis beams," *J. Opt. Soc. Am. A* **11**, 2516–2525 (1994).
16. G. Gouesbet, "Validity of the localized approximation for arbitrary shaped beams in the generalized Lorenz-Mie theory for spheres," *J. Opt. Soc. Am. A* **16**, 1641–1650 (1999).
17. K. F. Ren, G. Grehan, and G. Gouesbet, "Scattering of a Gaussian beam by an infinite cylinder in the framework of generalized Lorenz-Mie theory: formulation and numerical results," *J. Opt. Soc. Am. A* **14**, 3014–3025 (1997).
18. J. F. Owen, R. K. Chang, and P. W. Barber, "Internal electric field distributions of a dielectric cylinder at resonance wavelengths," *Opt. Lett.* **6**, 540–542 (1981).
19. D. S. Benincasa, P. W. Barber, J.-Z. Zhang, W.-F. Hsieh, and R. K. Chang, "Spatial distribution of the internal and near-field intensities of large cylindrical and spherical scatterers," *Appl. Opt.* **26**, 1348–1356 (1987).
20. C. F. Bohren and D. R. Huffman, *Absorption and Scattering of Light by Small Particles* (Wiley-Interscience, 1983).
21. E. D. Hirlleman and W. H. Stevenson, "Intensity distribution near a Gaussian laser beam focus," *Appl. Opt.* **17**, 3496–3499 (1978).